

Impulse-Radiating Antenna With an Offset Geometry

Kangwook Kim, *Member, IEEE*, and Waymond R. Scott, *Senior Member, IEEE*

Abstract—An offset impulse-radiating antenna (IRA) is numerically analyzed and compared with a typical centered IRA. In the typical centered IRA, the transverse electromagnetic (TEM) feed arms block the aperture because they are located at the center of the aperture. This blockage causes multiple reflections inside the antenna and, thus, ripples in the tail of the radiated waveform. In the offset IRA, the TEM feed arms are removed from the aperture, lowering the tail ripples caused by multiple reflections between the TEM feed arms and the reflector. The boresight gains and the impulse amplitudes are seen to be essentially the same for both IRAs. The monostatic radar cross section of the offset IRA is significantly lower than that of the centered IRA for the plane wave incident from the boresight direction because the wave incident to the offset IRA is diverted toward the focal point of the reflector, which is away from the boresight direction. The offset IRA has a shadow behind the reflector. This feature can be useful in bistatic radar applications because the antennas can be placed in the shadows of each other.

Index Terms—Impulse-radiating antennas (IRAs), offset reflector antennas, ultrawide-band (UWB) antennas.

I. INTRODUCTION

A typical impulse-radiating antenna (IRA) consists of a circular parabolic reflector and one or two pairs of conical transverse electromagnetic (TEM) feed arms whose apex is located at the focal point of the reflector (centered IRA) [1]–[5]. The TEM feed arms guide a spherical TEM wave originating at the apex toward the reflector. The reflector converts the spherical wave into an equi-phase aperture field, which is focused at infinity in the boresight direction. The resulting boresight radiation is an impulse-like waveform when the antenna is excited by a step pulse. This short-pulse radiating capability makes the IRA useful in many applications such as remote sensing, ultrawide-band weapons, and nondestructive testing [6]–[10].

One problem associated with the centered IRA, however, is the aperture blockage caused by the presence of the TEM feed arms in front of the reflector [11], [12]. The blockage causes the reduction in the impulse amplitude and multiple reflections inside the antenna. The multiple reflections cause ripples in the tail of the radiated waveform, which should be avoided in certain remote sensing applications. The blockage can be lessened by reducing the size of the TEM feed arms. However, this leads to the increase in the characteristic impedance of the TEM feed arms, making it difficult to match the antenna to the source [13]. Another method of reducing the blockage is using an offset geometry (offset IRA). This has been suggested in the literature

Manuscript received July 8, 2004; revised October 19, 2004. This work was supported in part by the U.S. Army RDECOM CERDEC Night Vision and Electronic Sensors Directorate, Countermine Division.

The authors are with the School of Electrical and Computer Engineering, Georgia Institute of Technology, Atlanta, GA 30332-0250 USA (e-mail: kangwook.kim@ece.gatech.edu; waymond.scott@ece.gatech.edu).

Digital Object Identifier 10.1109/TAP.2005.846808

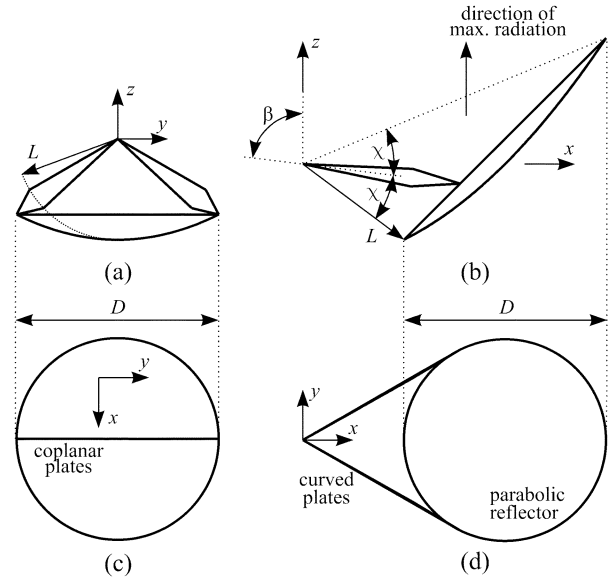


Fig. 1. Comparison of the geometries: (a), (c) diagrams of the centered IRA and (b), (d) diagrams of the offset IRA.

[3], [14], but has not been investigated. In this geometry, the TEM feed arms are tilted away from the aperture, and therefore the blockage can be minimized [15], [16].

In this paper, we investigate the characteristics of the offset IRA both in the frequency and the time domains. The frequency-domain results show the characteristics of the antenna independent of the input-pulse waveform. The time-domain results provide the basic idea of how the antenna operates and often show the advantages of the offset IRA more clearly. In Sections II and III, we discuss the advantages of the offset IRA over the centered IRA in detail, which include smaller tail ripples and lower RCS.

II. GEOMETRY

The geometries of the centered IRA and the offset IRA are compared in Fig. 1. In the figure, the reflector is a portion of a paraboloid that is carved out by the intersection of the paraboloid and a cone. The equation of the paraboloid in the rectangular coordinate system is

$$x^2 + y^2 = 4F(z + F), \quad (1)$$

where F is the focal length of the paraboloid. The paraboloid is rotationally symmetric with respect to the z -axis and has the focus at the coordinate origin. The equation of the cone is

$$\cos \chi \sqrt{x^2 + y^2 + z^2} = x \sin \beta - z \cos \beta, \quad (2)$$

where χ is the interior half angle of the cone, and β is the angle between the rotational axis of the cone and the z -axis. The angle

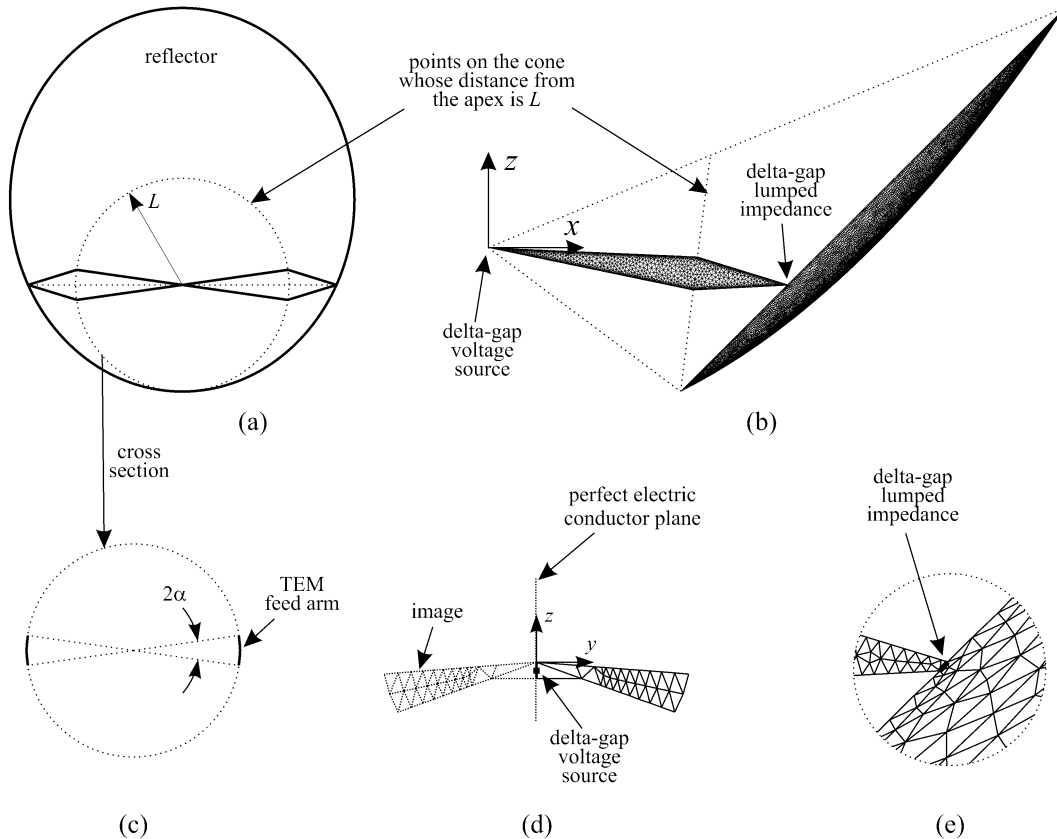


Fig. 2. (a) Diagram of the offset IRA when projected onto the plane normal to the axis of the cone. (b) Mesh for the numerical model of the offset IRA. (c) Cross section of the TEM feed arms at distance L from the apex. (d) Mesh around the electrically small resistor. (e) Mesh around the electrically small resistor. The TEM feed arms are curved along the surface of the cone. The angle 2α is 16.3° in the projected plane.

β is zero for the centered IRA. The intersection of the two surfaces is an ellipse and its projection onto the x - y plane is a circle whose equation is [17]

$$(x - x_0)^2 + y^2 = \left(\frac{D}{2}\right)^2 \quad (3)$$

where

$$x_0 = \frac{2F \sin \beta}{\cos \beta + \cos \chi}, \text{ and}$$

$$D = \frac{4F \sin \chi}{\cos \beta + \cos \chi}.$$

The reflector forms an aperture of diameter D , which is focused at infinity on the z -axis when it is fed a spherical TEM wave launched at the coordinate origin.

The spherical TEM wave is guided by a pair of TEM feed arms. A pair of conical coplanar plates is used in the centered IRA as TEM feed arms. Conical coplanar plates are advantageous in the centered geometry because they do not cause blockage in the geometrical optics sense. However, they cause significant aperture blockage in the offset geometry. Thus, in the offset IRA, a pair of conical curved plates [13], [18] is used as TEM feed arms because they can be made to cause almost no blockage. A diagram of the cross section of the conical curved plates is shown in Fig. 2(c).

In this paper, the focal length to diameter ratio has been chosen to be $F/D = 0.5$ for both IRAs, and the angles associated with the TEM feed arms are such that they form a spherical TEM transmission line with the characteristic impedance of

TABLE I
GEOMETRICAL PARAMETERS OF THE IRAS

	F/D	L/D	Z_c	β	TEM feed arms
Offset IRA	0.5	0.625	400Ω	82.9°	curved
Centered IRA	0.5	0.5	400Ω	0°	coplanar

400Ω . The geometrical parameters of the two IRAs are summarized in Table I, where Z_c is the characteristic impedance of the TEM feed arms.

Note that in both IRAs, the arms are conical within a sphere of radius L centered at the apex, where L is chosen to be the shortest distance from the apex to the reflector. Each arm is then linearly tapered and terminated with an electrically-small 200Ω resistor outside the spherical region so that the series resistance of one pair of TEM feed arms at zero frequency is 400Ω . Note that the spherical TEM wave launched at the apex propagates outwardly without a disturbance within the spherical region. The first possible disturbance is the negative reflection from the reflector. This will be compensated at the apex by the positive reflection from the taper [19].

To analyze the radiation characteristics of the IRAs, a numerical model has been built using EIGER, which is a method of moments code suite [20]. The mesh for the numerical model of the offset IRA is shown in Fig. 2(b)–(d). To reduce the computational load, symmetry is utilized, so only one half of the geometry is meshed. The results for the full geometry can be obtained from the results of the half geometry model by simple algebraic manipulations [15]. The electrically small resistors are modeled using a delta-gap lumped impedance model. The mesh

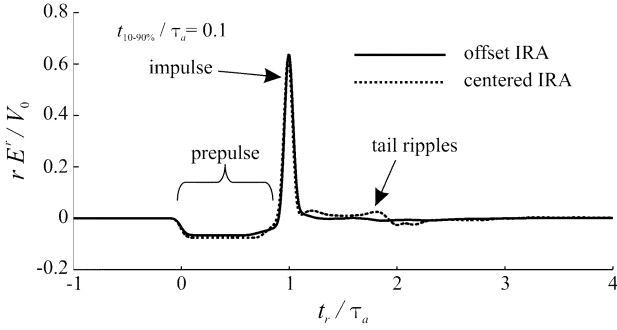


Fig. 3. Radiated field on boresight from the offset IRA (solid line) and the centered IRA (dotted line) for a step-like pulse with $t_{10-90\%}/\tau_a = 0.1$.

is excited by a delta-gap voltage source placed at the apex of the TEM feed arms. The numerical calculations are conducted on the Beowulf cluster at the Electromagnetics/Acoustics Laboratory at the Georgia Institute of Technology. The responses are obtained at 120 frequency points for the centered IRA and 150 frequency points for the offset IRA within a normalized frequency range of $D/\lambda = 0.102$ to $D/\lambda = 15.3$. The responses in the time domain are obtained using the Fourier transform technique. The total run times for the primary quantities (mesh currents) are approximately 74 hours for the centered IRA and 86 hours for the offset IRA using 32 computer nodes; each node is equipped with an AMD Athlon 2200+ processor. The performance of the numerical model has been validated in [21].

III. ANALYSIS

The primary motivation to use the offset geometry is to lower the tail ripples in the radiated waveform. Fig. 3 shows the radiated waveforms on boresight as functions of retarded time $t_r = t - r/c$ for the step-like pulse

$$V_t = V_0 \left\{ \frac{1}{2} + \frac{1}{2} \operatorname{erf} \left(k_1 \frac{t}{t_{10-90\%}} \right) \right\},$$

$$k_1 = 2 \operatorname{erf}^{-1}(0.8) \simeq 1.8124 \quad (4)$$

where $\operatorname{erf}(t)$ is the error function, and $t_{10-90\%}$ is the 10%–90% rise time of the step-like pulse [22]. Here, the input pulse is incident in the 400Ω transmission line, and the input pulse rise-time is $t_{10-90\%} = 0.1\tau_a$, where $\tau_a = D/c$ is the time required by light to travel the length of the aperture diameter. For this input pulse, the aperture is roughly 10 times as long as the leading edge of the pulse. The figure shows that the offset IRA has a smaller and simpler tail waveform than the centered IRA. This is because the TEM feed arms are mostly removed from the aperture in the offset IRA, which causes the amplitude of the multiple reflections between the TEM feed arms and the reflector to be significantly reduced, and therefore the radiation from the multiple reflections is reduced. The figure shows that the impulse amplitudes are essentially the same. The prepulse amplitudes are slightly different because of the difference in the TEM feed arm geometries.

Because the impulse amplitudes for the two IRAs are essentially the same, and the radiated energy is mostly contained in the impulse, the gain on boresight must be comparable. Fig. 4 shows the gains of the two IRAs and a uniformly illuminated

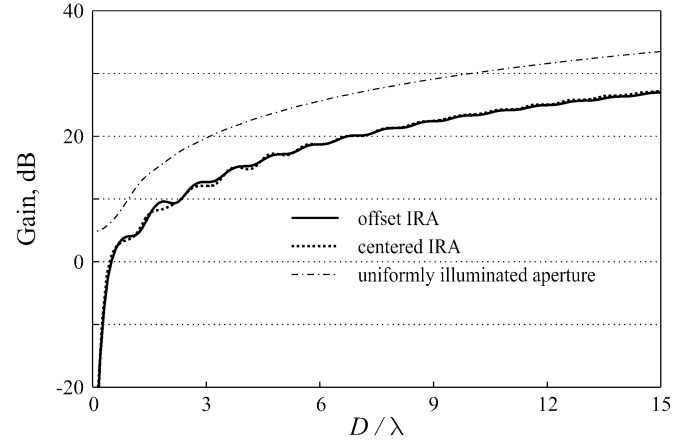


Fig. 4. Gain versus frequency for the offset IRA (solid line), centered IRA (dotted line), and the uniformly illuminated aperture (dash-dot line).

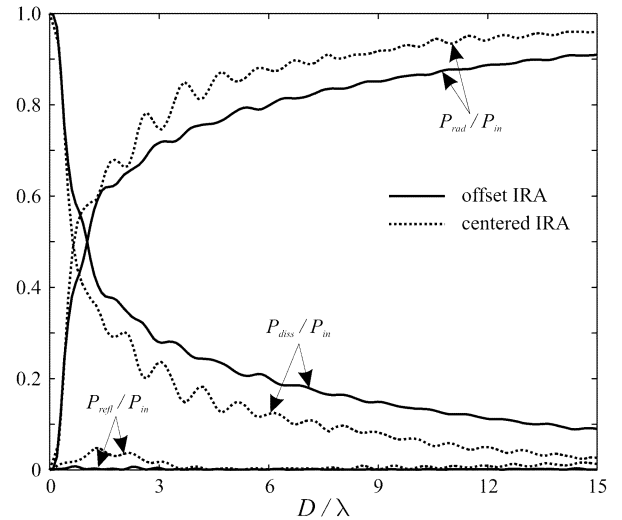


Fig. 5. Power budgets of the offset IRA (solid line) and centered IRA (dotted line).

aperture on boresight plotted as a function of frequency. Here the gain for the two IRAs is defined as

$$\text{Gain} = 4\pi \frac{U_0}{P_{in}} \quad (5)$$

where U_0 is the radiation intensity on boresight, and P_{in} is the power incident in the transmission line. The power radiated by the uniformly illuminated aperture is assumed to be equal to P_{in} .

Fig. 4 shows that the gain on boresight is essentially the same for both IRAs as it is expected. The small ripples in the gains for the IRAs are due to the direct radiation from the TEM feed arms (prepulse). Note that the gains for the IRAs are approximately 6 dB lower than that of the uniformly illuminated aperture at most frequencies (25% aperture efficiency). This loss is mostly due to the spill over and nonuniform aperture illumination (amplitude and polarization) [23]–[25]. At frequencies lower than $D/\lambda < 0.5$, the gains for both IRAs are less than 0 dB because the incident power is mostly dissipated in the resistors at the junctions between the TEM feed arms and the reflector.

One may be interested in the power budgets of the IRAs to see how much of the incident power is eventually radiated or dissipated in the resistors. The power budgets are plotted against frequency in Fig. 5. The figure shows the power reflected back

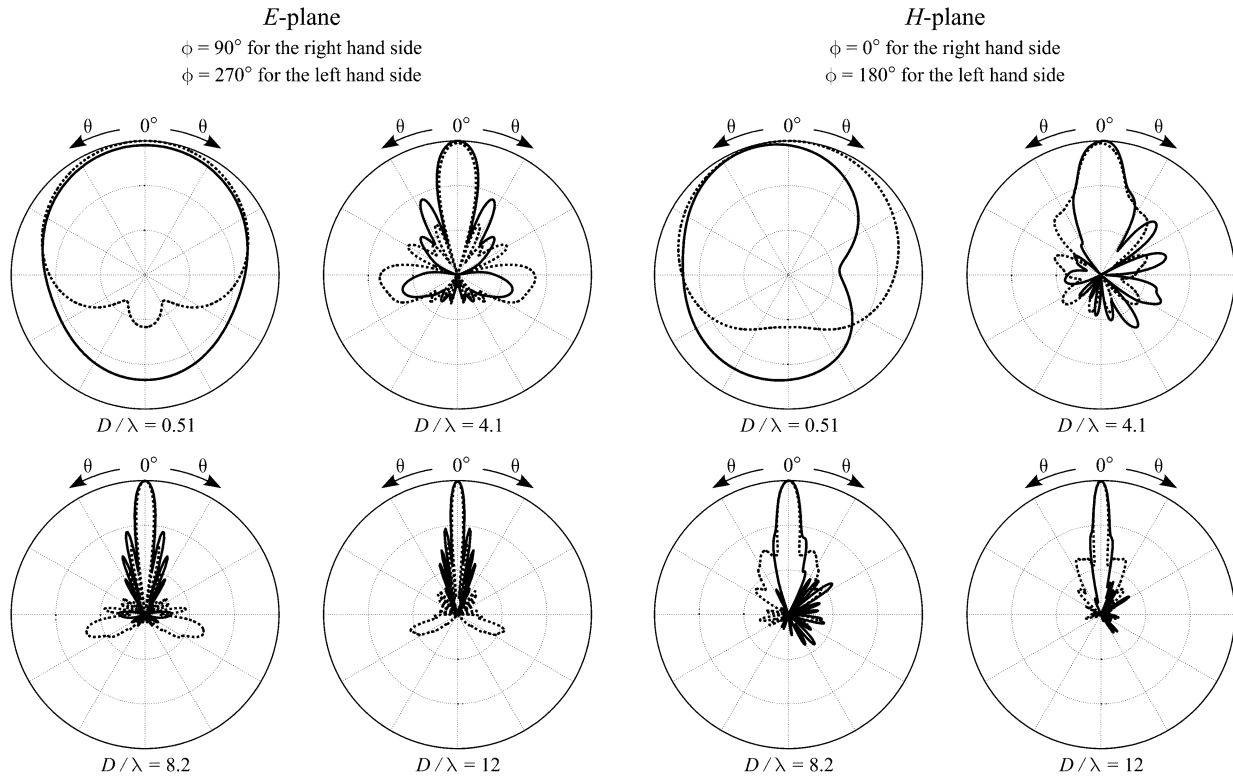


Fig. 6. Radiation patterns of the offset IRA (solid line) and centered IRA (dotted line) at four frequencies. The patterns are plotted in dB-scale (0 to -30 dB) relative to the maximum of both antennas at each frequency. In the E -plane, $\phi = 90^\circ$ and 270° for the right and left halves of each graph, respectively. In the H -plane, $\phi = 0^\circ$ and 180° for the right and left halves of each graph.

in the transmission line (P_{refl}), power dissipated in the resistors (P_{diss}), and the power radiated in free space (P_{rad}). For both IRAs, P_{diss} dominates at low frequencies, and P_{rad} dominates at high frequencies. Thus, the radiation efficiency of the IRAs improves with increasing frequency. The reflected powers for both IRAs are small over the entire frequency range shown in the figure because both IRAs are well-matched to the 400Ω transmission line. Note that the centered IRA is seen to radiate more power and dissipate less power than the offset IRA at most frequencies. Because the gain on boresight of the two IRAs were essentially the same, the figure implies that the offset IRA radiates less in the off-boresight directions than does the centered IRA, which is a desired characteristic in many applications, such as ultrawide-band weapons and remote sensing.

Shown in Fig. 6 are the radiation intensity patterns of the antennas in the principal E - and H -planes at four frequencies. The radiation intensities are normalized by the maximum radiation intensity of both IRAs at each frequency and plotted on a 30 dB scale. The figure shows that the directivity increases with increasing frequency for both IRAs. The offset IRA has a slightly broader main beam than the centered IRA, and the sidelobe distributions are different. For example in the E -plane, the first sidelobes of the offset IRA are somewhat larger than those of the centered IRA, and the backward radiation of the offset IRA is smaller than that of the centered IRA. The differences in the sidelobe distribution may give one antenna an advantage over the other depending on the application. The sidelobes of the offset IRA in the $\phi = 0^\circ$ direction in the H -plane are believed to be due to the wave creeping around the back of the

reflector, which may be reduced by an appropriate treatment of the reflector edge.

Fig. 6 shows that at the low frequency ($D/\lambda = 0.51$), the offset IRA radiates less around ($\theta = 90^\circ, \phi = 0^\circ$), and the centered IRA radiates less around $\theta = 180^\circ$. These directions are shadowed by the reflectors. However, at high frequencies, the offset IRA radiates more behind the reflector than toward other off-boresight directions. Thus, in order to determine the locations of the antenna support structure and other equipment, it may be useful looking at the radiated waveform in the time domain.

Fig. 7 shows the the radiated E -fields of the IRAs as functions of time for a step-like pulse with $t_{10-90\%}/\tau_a = 0.1$. The impulse is clearly defined only in the boresight direction, because the impulse spans an ultra-wide range of frequency, and the beam width for the high-frequency components are narrow. In other directions, the waveforms are distorted. The amplitudes are seen to be dominated by the low-frequency radiation pattern. The reason for this is that the input pulse, i.e., step-like pulse, has a large amount of low frequency contents. Because the IRA is usually excited by a step-like pulse, the best place to keep the support structure and other equipment may be behind the reflector. However, the backward radiation of the offset IRA at lower frequencies ($D/\lambda = 0.51$) may be problematic for certain applications.

Fig. 5 showed that both IRAs are well-matched to the 400Ω transmission line. This can be confirmed by looking at the voltage standing wave ratio (VSWR), which is plotted as a function of frequency in Fig. 8 for a 400Ω transmission line. The

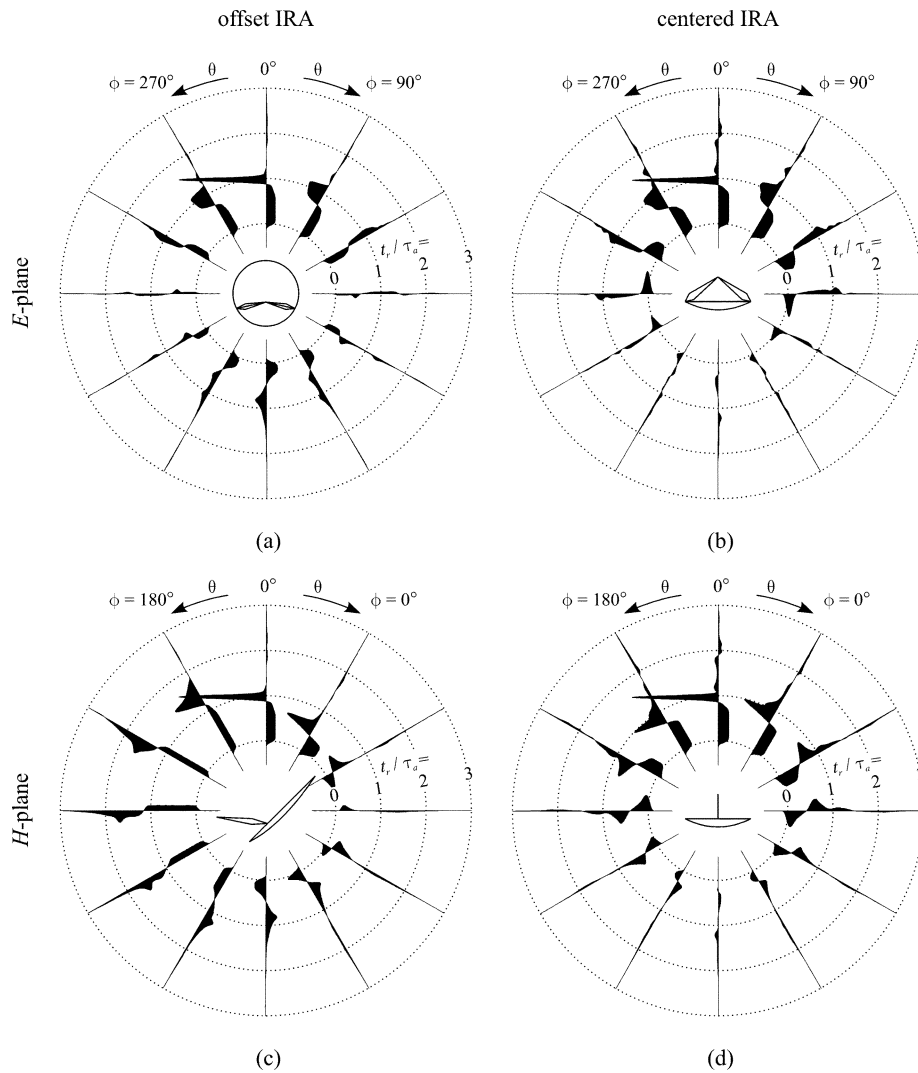


Fig. 7. Radiated E -fields of the offset IRA and the centered IRA for a step-like pulse with $t_{10-90\%}/\tau_a = 0.1$ (a), (b) Radiated fields in the E -plane. (c), (d) Radiated fields in the H -plane. The orientation of the antenna is shown at the center of each figure.

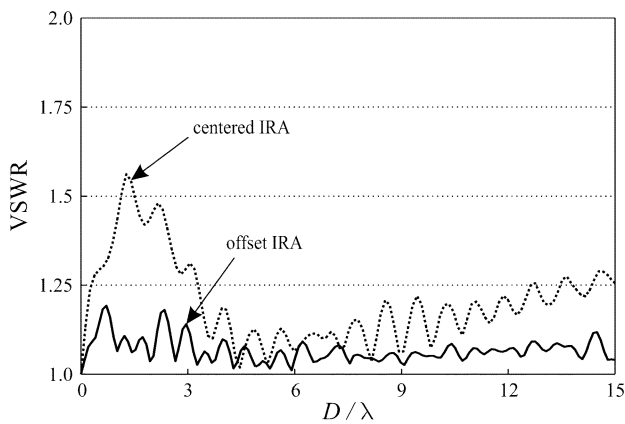


Fig. 8. Voltage standing wave ratios of the offset IRA (solid line) and centered IRA (dotted line) at four frequencies.

figure shows that the VSWR is much less than 2.0, and the two IRAs are well-matched to the transmission line. The VSWR of the centered IRA is higher than that of the offset IRA at most frequencies. The reason for this is that the TEM feed arms are

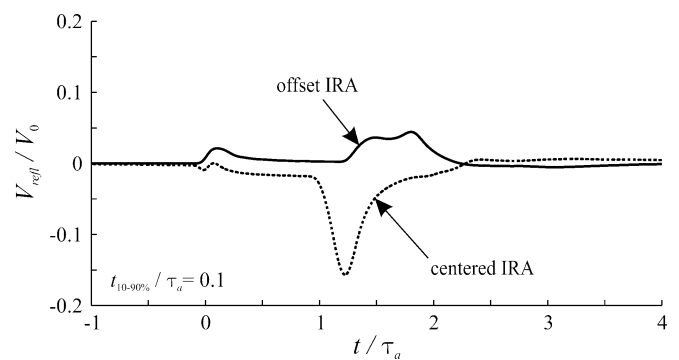


Fig. 9. Reflected voltage waveforms in the transmission line for the offset IRA (solid line) and centered IRA (dotted line) for a step-like pulse with $t_{10-90\%}/\tau_a = 0.1$.

better terminated at the reflector in the offset IRA than they are in the centered IRA.

Fig. 9 shows the reflected voltage waveforms in the transmission line as functions of time. The figure shows the reflection from the TEM feed arm terminations at $t/\tau_a \approx 1$ for the centered IRA and at $t/\tau_a \approx 1.25$ for the offset IRA. Note that

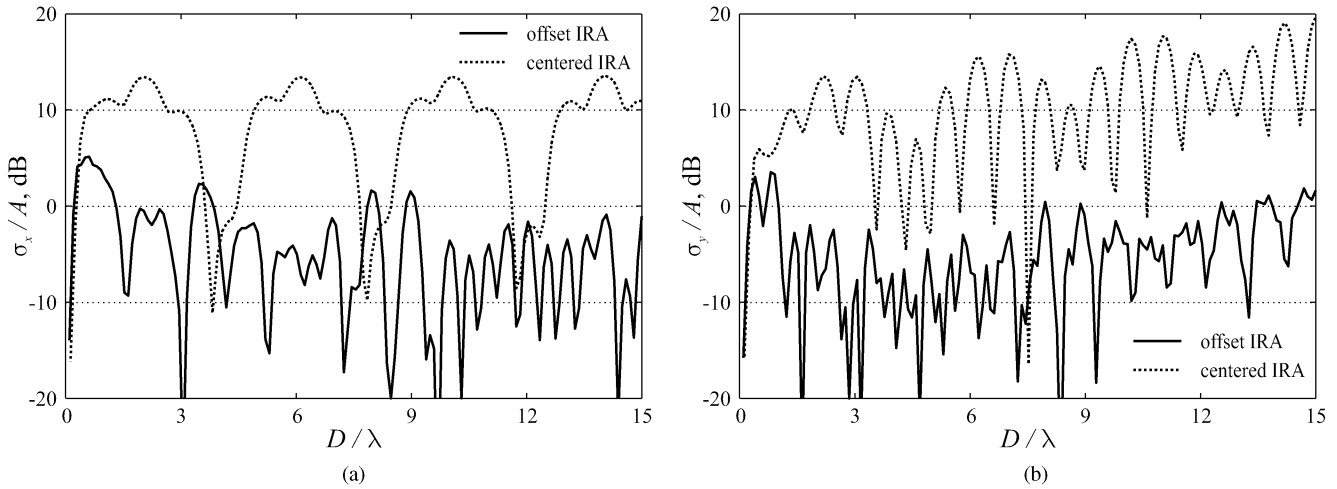


Fig. 10. Radar cross sections of the offset IRA (solid line) and the centered IRA (dotted line) (a) for the x -polarized plane wave and (b) for the y -polarized plane wave.

the TEM feed arms of both IRAs are linearly tapered to cancel the signal from the reflector [19]. The cancellation is seen to be more effective in the offset IRA than in the centered IRA. In the figure, the first reflection at $t/\tau_a \simeq 0$ is due to the approximation made to the apex geometry. The first possible disturbance after this reflection is the signal from the TEM feed arm taper. However, the waveform is not exactly zero between the signal from the apex and the signal from the TEM feed arm taper. This is due to the small error in the characteristic impedance of the TEM feed arms predicted by the numerical model. The errors are less than 1% and 5% for the offset and centered IRAs, respectively.

The low VSWR is particularly important in remote sensing applications, such as the ground-penetrating radar (GPR) systems, where the ringing inside the transmission line can obscure the signal from a target nearby the antenna. In such applications, the signal from the target can also be obscured by the multiple reflections between the ground and the antenna. To lower this type of multiple reflections, the antenna should minimally reflect the wave from the ground back toward the ground. The amount of power that is reflected toward the ground by the antenna may be estimated by the monostatic radar cross section (RCS) in the boresight direction. Fig. 10 shows the monostatic RCS's when the antennas are illuminated by a unit-amplitude plane wave. In the figure, the RCS is normalized by the aperture area $A = \pi(D/2)^2$. The incident plane wave is \hat{x} -polarized in Fig. 10(a) and \hat{y} -polarized in Fig. 10(b). For these graphs, a 400 Ω lumped resistor is placed at the apex of the TEM feed arms for each IRA to simulate the 400 Ω transmission line. The figure shows that the RCS of the offset IRA is significantly lower than that of the centered IRA at most frequencies. The reason for this is that the incident wave is diverted toward the apex of the TEM feed arms by the reflector of the offset IRA. The low RCS and the radiated waveform pattern of the offset IRA shown in Figs. 7 and 10 suggest the bistatic configuration of the offset IRA for use in GPR systems, where the antennas are placed side by side looking in the same direction (Fig. 11). In such systems, the coupling between the antennas may be reduced by placing two offset IRAs in the shadows of each other.

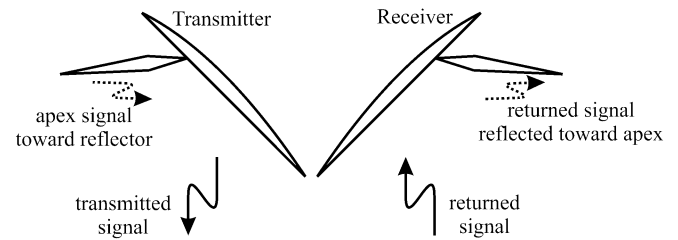


Fig. 11. Suggested configuration for bistatic radar systems.

IV. CONCLUSION

An offset IRA was numerically analyzed and compared with a centered IRA. In the offset IRA, the TEM feed arms were removed from the aperture to reduce the multiple reflections between the TEM feed arms and the reflector. The offset IRA was shown to have smaller and simpler tail ripples in the boresight radiated waveform while the impulse amplitude was essentially the same.

The offset IRA showed other improvements. First, the monostatic RCS for the boresight illumination was greatly lowered because the incident wave from the boresight direction is diverted toward the apex which is away from the boresight direction. This low RCS may be useful especially in the near-field sensing applications, such as the ground-penetrating radar systems. Note that in the near-field region, the impulse is not fully developed, so the performance of the IRA for such applications is degraded. This may be overcome to some degree by using an ellipsoidal reflector instead of a parabolic reflector [10].

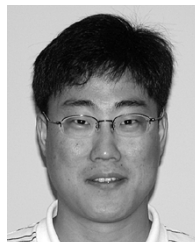
Second, the asymmetric radiation pattern may be useful in bistatic radar systems because the antennas can be placed where the radiation is minimal. Finally, the offset IRA was shown to have a lower VSWR than the centered IRA. The lower VSWR was due to the effective cancellation of the reflector signal by the signal from the TEM feed arm taper. It may be worth investigating the optimal taper profile for the TEM feed arm to lower the reflected voltage. Other methods of TEM feed arm termination may be worth investigating as well. For example, Abdalla *et al.* improved the VSWR by terminating each TEM

feed arm with a number of resistors placed in a series-parallel combination in [26]. Their approach is particularly appealing in high power applications, where P_{diss} is dissipated in a number of lumped resistors rather than a single lumped resistor; therefore, the breakdown of the resistors is prevented.

Note that one advantage of the centered IRA is that one can add a second pair of TEM feed arms to the centered IRA to lower the input impedance [21], [27]. The offset IRA geometry does not allow the second pair of TEM feed arms so it will be more difficult to match the offset IRA to the source because of its higher impedance. Another disadvantage of the offset IRA is that it uses a bigger reflector to achieve essentially the same gain as the centered IRA.

REFERENCES

- [1] C. E. Baum and E. G. Farr *et al.*, "Impulse radiating antennas," in *Ultra-Wideband, Short Pulse Electromagnetics*, H. Bertoni *et al.*, Eds. New York, Plenum, 1993, pp. 139–147.
- [2] E. G. Farr, C. E. Baum, and C. J. Buchenauer, "Impulse radiating antennas, part II," in *Ultra-Wideband, Short Pulse Electromagnetics 2*, L. Carin and L. B. Felsen, Eds. New York, Plenum, 1995, pp. 159–170.
- [3] C. E. Baum, "Radiation of impulse-like transient fields," *Sensor and Simulation Notes #321*, Nov. 1989.
- [4] C. E. Baum, E. G. Farr, and D. V. Giri, "Review of impulse-radiating antennas," in *Revis of Radio Science 1996–1999*, W. R. Stone, Ed. Oxford, U.K.: Oxford Univ. Press, 1999, ch. 16, pp. 403–439.
- [5] L. H. Bowen, E. G. Farr, C. E. Baum, T. C. Tran, and W. D. Prather, "Experimental results of optimizing the location of feed arms in a collapsible IRA and a solid IRA," *Sensor and Simulation Notes #450*, Nov. 2000.
- [6] M. H. Vogel, "Design of low-frequency compensation of an extreme-bandwidth TEM horn and lens IRA," *Sensor and Simulation Notes #391*, Apr. 1996.
- [7] F. M. Tesche, "Some considerations for the design of pulse-radiating antennas," *Sensor and Simulation Notes #398*, Jul. 1996.
- [8] D. V. Giri, H. Lackner, I. D. Smith, D. W. Morton, C. E. Baum, J. R. Marek, W. D. Prather, and D. W. Scholfield, "Design, fabrication, and testing of a paraboloidal reflector antenna and pulser system for impulse-like waveforms," *IEEE Trans. Plasma Sci.*, vol. 25, pp. 318–326, Apr. 1997.
- [9] J. B. Rhebergen, A. P. M. Zwamborn, and D. V. Giri, "Design of an ultra-wideband ground-penetrating radar system using impulse radiating antennas," in *Proc. 2nd Int. Conf. the Detection of Abandoned Land Mines*, Oct. 1998, pp. 45–49.
- [10] K. Kim and W. R. Scott Jr, "Analysis of impulse-radiating antennas with ellipsoidal reflectors," *Sensor and Simulation Notes #481*, Oct. 2003.
- [11] Y. Rahmat-Samii, "Analysis of blockage effects on TEM-fed paraboloidal reflector antennas," *Sensor and Simulation Notes #347*, Oct. 1992.
- [12] Y. Rahmat-Samii and D. W. Duan, "Axial feed of a TEM-fed UWB reflector antenna: The PO/PTD construction," *Sensor and Simulation Notes #363*, Dec. 1993.
- [13] E. G. Farr, "Optimizing the feed impedance of impulse radiating antennas, part I: Reflector IRAs," *Sensor and Simulation Notes 354*, Jan. 1993.
- [14] C. E. Baum, "Variations on the impulse-radiating antenna theme," *Sensor and Simulation Notes #378*, Feb. 1995.
- [15] K. Kim, "Numerical and experimental investigation of impulse-radiating antennas for use in sensing applications," Ph.D. dissertation, Georgia Inst. Technology, Atlanta, GA, 2003.
- [16] K. Kim and W. R. Scott Jr, "Analysis of an offset impulse-radiating antenna," *Sensor and Simulation Notes #476*, Jun. 2003.
- [17] V. Jamnejad-Dailami and Y. Rahmat-Samii, "Some important geometrical features of conic-section-generated offset reflector antennas," *IEEE Trans. Antennas Propag.*, vol. AP-28, pp. 952–957, Nov. 1980.
- [18] E. G. Farr, "Optimization of the feed impedance of impulse radiating antennas. Part II: TEM horns and lens IRAs," *Sensor and Simulation Notes #384*, Nov. 1995.
- [19] C. E. Baum, "Some topics concerning feed arms of reflector IRAs," *Sensor and Simulation Notes #414*, Oct. 1997.
- [20] R. M. Sharpe, J. B. Grant, N. J. Champagne, W. A. Johnson, R. E. Jorgenson, D. R. Wilton, W. J. Brown, and J. W. Rockway, "EIGER: Electromagnetic interactions generalized," in *IEEE AP-S Int. Symp. Dig.*, Quebec, Canada, Jul. 1997, pp. 2366–2369.
- [21] K. Kim and W. R. Scott Jr, "Numerical analysis of the impulse-radiating antenna," *Sensor and Simulation Notes #474*, Jun. 2003.
- [22] M. Abramowitz and I. A. Stegun, *Handbook of Mathematical Functions with Formulas, Graphs, and Mathematical Tables*. New York, Dover, 1972.
- [23] C. J. Buchenauer, J. S. Tyo, and J. S. H. Schoenberg, "Aperture efficiencies of impulse radiating antennas," *Sensor and Simulation Notes #421*, Nov. 1998.
- [24] —, "Aperture efficiencies of impulse radiating antennas," in *Ultra-Wideband, Short Pulse Electromagnetics 4*, H. Bertoni *et al.*, Eds. New York, Plenum, 1999, pp. 91–108.
- [25] C. J. Buchenauer and J. S. Tyo, "Prompt aperture efficiencies of impulse radiating antennas with arrays as an application," *IEEE Trans Antennas Propag.*, vol. 49, no. 8, pp. 1155–1165, Aug. 2001.
- [26] M. Abdalla, M. Skipper, D. V. Giri, H. V. La, T. Smith, D. McLemore, J. Burger, R. Torres, T. Tran, W. Prather, and C. E. Baum, "Evaluation of the terminating impedance in the conical-line feed of the 6-foot IRA," *Prototype IRA Memos #8*, Apr. 2001.
- [27] C. E. Baum, "Configuration of TEM feed for an IRA," *Sensor and Simulation Notes #327*, Apr. 1991.



Kangwook Kim (S'99–M'03) received the B.S. degree in electrical engineering from Ajou University, Korea, in 1997, and the M.S. (ECE) and Ph.D. (ECE) degrees from the Georgia Institute of Technology, Atlanta, in 2001 and 2003, respectively. His Ph.D. research was on the design, analysis, and measurement of pulse-radiating antennas.

He joined the faculty of the School of Electrical and Computer Engineering at the Georgia Institute of Technology in 2003 as a Postdoctoral Fellow. His current research interests include remote sensing of concealed objects, ultrawide-band electromagnetics, and pulsed antennas.



Waymond R. Scott (M'85–SM'03) was born in Calhoun, GA, on April 6, 1958. He received the B.E.E., M.S.E.E., and Ph.D. degrees from the Georgia Institute of Technology, Atlanta, in 1980, 1982, and 1985, respectively.

From 1979 to 1980, he was a Student Assistant and Graduate Research Assistant at the Georgia Tech Research Institute, and from 1980 to 1985, he was a Graduate Research Assistant in the School of Electrical Engineering at the Georgia Institute of Technology, where he is currently a Professor of Electrical and Computer Engineering. His research interest include methods for detecting buried objects using both electromagnetic and acoustic waves, measurement of the electromagnetic properties of materials, transient electromagnetic fields, and numerical methods including the finite element and the finite-difference time-domain techniques.